From medical imaging to computer simulation of Fractional Flow Reserve in four coronary artery trees

Simone Melchionna*[a], Stefania Fortini[a], Massimo Bernaschi[b], Mauro Bisson[b], Nahyup Kang[c], Hyong-Euk Lee[c]
[a]IPCF - CNR, Consiglio Nazionale delle Ricerche, P.le A. Moro 2, 00185 Rome, Italy; [b]IAC - CNR, Consiglio Nazionale delle Ricerche, Via dei Taurini 1, 00185 Rome, Italy; [c]Multimedia Processing Lab., Samsung Advanced Institute of Technology, South Korea

ABSTRACT

We present the results of a computational study of coronary trees obtained from CT acquisition at resolution of 0.35mm x 0.35mm x 0.4mm and presenting significant stenotic plaques. We analyze the cardiovascular implications of stenotic plaques for a sizeable number of patients and show that the standard clinical criterion for surgical or percutaneous intervention, based on the Fractional Flow Reserve (FFR), is well reproduced by simulations in a range of inflow conditions that can be finely controlled. The relevance of the present study is related to the reproducibility of FFR data by simulating the coronary trees at global level via high performance simulation methods together with an independent assessment based on *in vitro* hemodynamics. The data show that controlling the flow Reynolds number is a viable procedure to account for FFR as heart-cycle time averages and maximal hyperemia, as measured *in vivo*. The reproducibility of the clinical data with simulation offers a systematic approach to measuring the functional implications of stenotic plaques.

Keywords: Hemodynamics; Fractional Flow Reserve; Atherosclerotic plaques; High-Performance computing; Segmentation to Simulation pipeline; *In vitro* analysis.

1. INTRODUCTION

Coronary artery disease (CAD) can lead to significant reductions of the lumen and a atherosclerotic lesion may have far-reaching consequences on the global coronary circulation and blood supply to the myocardium. While coronary angiography is to date the most accurate morphologic assessment of the lumen of coronary arteries, the functional repercussions of significant coronary narrowing cannot be evaluated by imaging alone. Coronary anatomy and physiology interplay to a great extent since in conditions of ischemia, the coronary circulation has a significant capacity to adapt in order to provide adequate supply to the myocardium. Flow readjustment in vessels both distal and proximal to the lesion is achieved by controlling vascular smooth muscle tone (including autonomic control of microvascular resistance) and the development of collateral flow pathways from one well-supplied portion of the network to another portion hampered by CAD.

The presence of diffuse or focal stenotic plaques significantly affects not only the flow, but also the pressure distribution over a long-ranged portion of the coronary system. Fractional Flow Reserve (FFR) is a sensitive, reproducible measure of the functional significance of CAD in the catheterization laboratory [1]. FFR is the ratio of distal pressure versus that proximal to an atherosclerotic lesion, measured simultaneously as the average (across heart beats) pulsatile pressures. In recent years, the increasing positive clinical outcomes of FFR-guided treatment and substantial lowering of healthcare expenditure led to the incorporation of FFR into coronary revascularization guidelines by recommending its clinical use. FFR is now recommended by universal guidelines for detection of ischemia-related lesions when there is a paucity of other objective evidence for ischemia attributed to a specific lesion.

Medical Imaging 2014: Computer-Aided Diagnosis, edited by Stephen Aylward, Lubomir M. Hadjiiski,
Proc. of SPIE Vol. 9035, 903535 · © 2014 SPIE · CCC code: 1605-7422/14/$18 · doi: 10.1117/12.2043236

In catheter lab practice, FFR is acquired during maximal hyperemia [2] induced by pharmacological stress, that is, when myocardial blood flow requirements are maximal due to a substantial reduction of the peripheral resistance. In fact, maximal vasodilatation is crucial since pressure differences at rest do not provide significant variation of pressure and FFR. The end result is an extremely reproducible measure since the microvasculature has an extraordinary capability to vasodilate repeatedly to the same extent. By neglecting small pressure losses arising in healthy vessels, the normal FFR is virtually equal to unity while in pathologic cases, a measured FFR $\leq$ 0.75-0.80 is a sensitive indicator of a hemodynamically significant lesion. In clinical decision, FFR is considered to have a well-defined cut-off value, with a narrow "grey zone" between 0.75 and 0.80. Stenoses with an FFR below 0.75 (above a 25% pressure loss) almost invariably correlate with myocardial ischemia while FFR above 0.80 almost never associates with exercise-induced ischemia.

By accounting for both the subtended myocardial flow demand and the complete blood flow dedicated to the myocardial territory, FFR is a functional indication of an individual atherosclerotic lesion. In a normal epicardial coronary artery the pressure drop across a significant stenosis is negligible and blood flow is driven by the difference in pressure between the aorta and the distal myocardial pressure. In a functionally significant stenosis, blood flow significantly reflects the physiological response of the myocardium to the arterial narrowing [3]. However, one of reasons why FFR has become so attractive is the fact that FFR is not influenced by systemic hemodynamics conditions, such as systemic pressure, heart rate and left ventricular contractility [1].

In order to design preventive, diagnostic and therapeutic solutions, computer simulation is now becoming an important aid to cardiovascular medicine, in particular by offering new non-invasive routes to diagnose CAD. The upsurge of computational medicine is marking major progress due to the fact that blood flow can be determined to a satisfactory degree of accuracy even in realistically complex three-dimensional geometries [4]. Computer reconstructed FFR is based on anatomic data acquired from coronary artery CT scans to create a three-dimensional multi-branched model of the vessels [5, 6]. By reproducing the blood flow pattern within the anatomical model, it is then possible to determine the blood flow rate and pressure locally within the vessels, in a virtual analogue of a catheter-based measurement, and conveying the predictions of the hemodynamic simulations.

The present study evaluates FFR on a set of four patients in comparison with clinically measured FFR. Such a reduced, but significant, set of patients allows assessing the reproducibility of clinical FFR and, since the clinical FFR range in the 0.70-0.90% interval, this is a good assessment of the sensitivity of the methodology. This is an important step to evaluate the capabilities of the computational protocol, from the image segmentation process to the actual simulation, together with the accessory boundary conditions.

The simulation technology is based on the MUPHY software and on describing blood based from a multiscale biomechanical standpoint. MUPHY represents blood as a suspension of red blood cells in plasma and reproduces the flow at physiological hematocrit level. Most importantly, as the computer simulation lacks a direct incorporation of the microvasculature but rather uses an effective representation of the vascular periphery, this study determines the effect of such modeling conditions and the possible presence of systematic bias on the reconstructed FFR.

As a direct comparison of the local flow pattern *in vivo* presents technological limitations, the present study discusses the *in vitro* determination of blood flow and pressure. Such direct comparison between *in vivo* and *in silico* data is a crucial prerequisite to assess the quality of both approaches. In fact the *in vitro* analysis provides for the possible lack of the fluid dynamic validation between the *in silico* and *in vivo* data; moreover it can help assessing the origin of the anomalies by addressing the flow dynamics in the specific anatomic district. In addition, since the *in vitro* fluid-dynamic set-up is based on a protocol similar to the computational one, this provides a direct control on the factors influencing hemodynamics.

2. METHODS

The computer simulations are based on anatomies of the coronary systems acquired from a clinical coronary Computed Tomography Angiography (CTA) examination and reconstructed after acquisition using a 0.35mm x 0.35mm detector row CT scanner (SIEMENS SOMATOM Definition Flash). The evaluation in this work was approved by the Samsung

Medical Center, where the clinical images were acquired. Written informed consent from the patients was waived to share their imaging data for medical research. The dataset is composed by three left (P1, P2 and P4) and one right (P3) coronary anatomies.

The angiographic images are segmented using the software developed by our team into a stack of two-dimensional lumen contours orthogonal to the segmented vessel centerlines at a nominal spacing of 0.5 mm. Given the current CT resolution, the reconstructed anatomies consider only coronary arteries that can be accurately detected by the imaging technique, i.e., only those vessels with diameter larger than 0.5 mm and the vessels were truncated when their diameter fell below this value. An example of the segmentation result is shown in Figure 1 and refers to the P2 case: the A plot is related to the computational model whereas the B plot is the *in vitro* model.

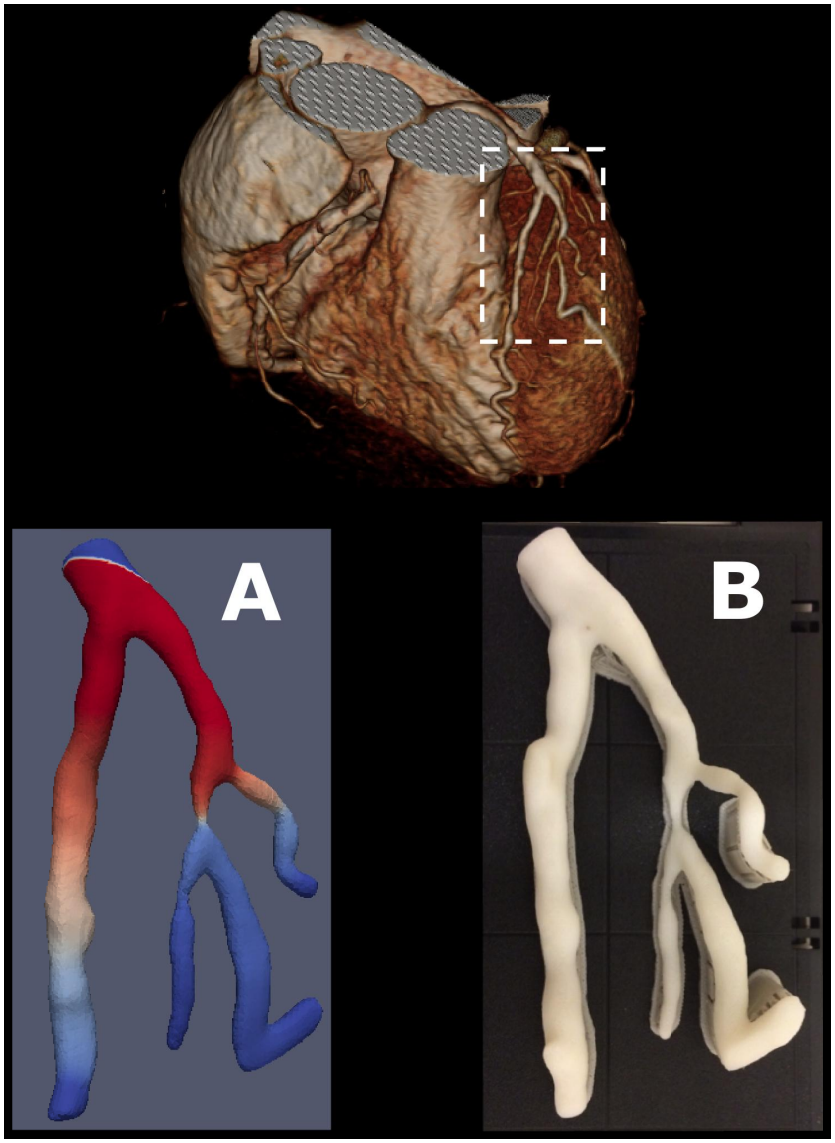

Figure 1: segmentation result for the coronary anatomy P2; A is the computational model, B is the *in vitro* model

For each coronary tree, the reconstructed anatomy comprises one inlet, departing from the aorta, and a variable number of outlets, as illustrated in Figure2.

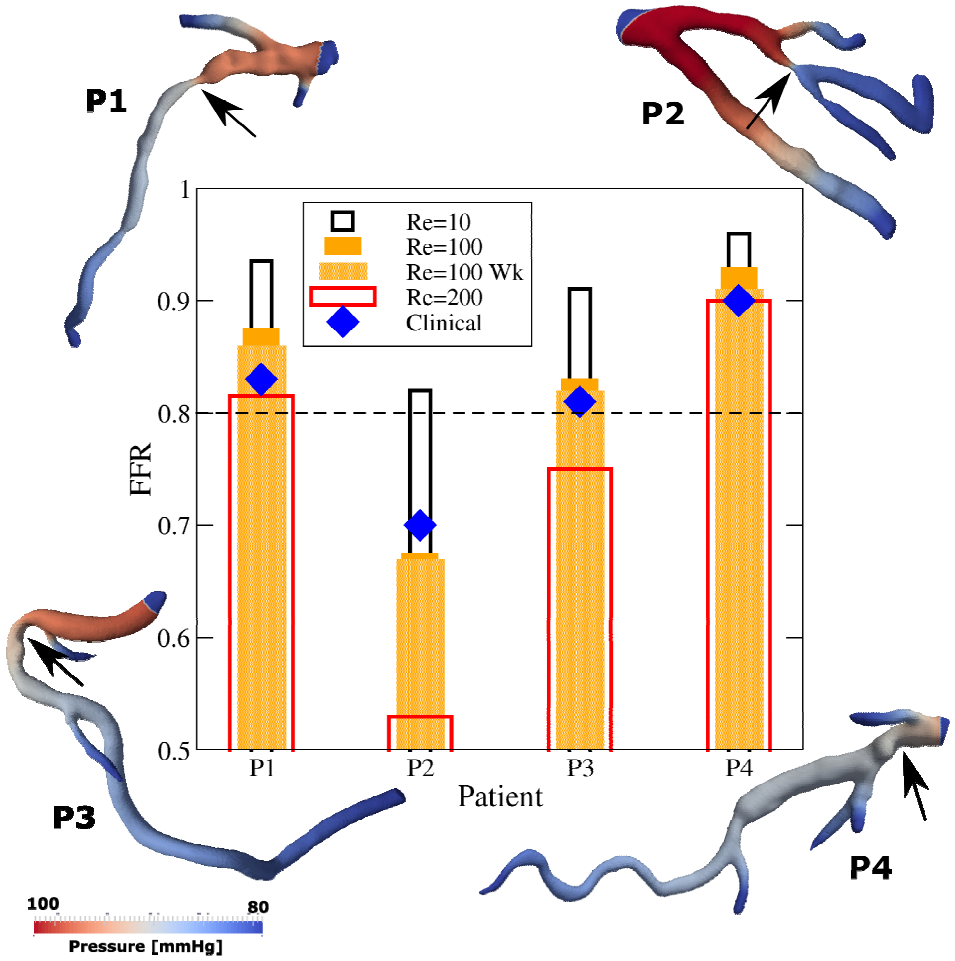

Figure 2: FFR as obtained in simulations for different coronary systems. The lateral figures show the P1-P4 coronary systems, colored according to the local pressure. The central plot reports the simulated FFR as compared to the clinical one. Black: Re=10, orange: Re=100, pale orange: Re=100 with peripheral resistance (Windkessel model), red: Re=200. The clinical data are shown as blue diamonds. The dashed line at FFR=0.8 marks cases for putative revascularization.

The segmentation is achieved by selecting the reference radiodensity of 300 HU, and a radiation window of 20 HU. During the segmentation process, the geometries were regularized according to a linear filter (level-three smoothing) to minimize artifacts in the fluid dynamics due to the various forms of uncertainty in the imaging data such as noise, artifact introduced by CT imaging, and imperfect coronary segmentation.

The simulation methodology combines the Lattice Boltzmann method (LBM) to reproduce the dynamics for the blood plasma with the explicit motion of red blood cells. LBM is a computational approach to simulate blood flows [7] in

generic vascular geometries. It further explicitly handles the motion of suspended bodies to determine the arrangement of red blood cells in large-scale simulations together with their effect in the hemodynamics, from affecting the local flow pattern to the global biomechanics, as described in [8]. In essence, in the LBM blood plasma is described via the "populations" $f_p(\vec{x},t)$ representing the probability of finding plasma molecules at given position $\vec{x}$ and time t and moving along a discrete direction p. The populations are represented over a mesh and evolve as

$$\boldsymbol{f_p}\left(\vec{\boldsymbol{x}}+\vec{\boldsymbol{c}}_{\boldsymbol{p}},\boldsymbol{t}+\boldsymbol{1}\right)=\boldsymbol{\omega f_p^{eq}}(\vec{\boldsymbol{x}},\boldsymbol{t})+(\boldsymbol{1}-\boldsymbol{\omega})\boldsymbol{f_p}(\vec{\boldsymbol{x}},\boldsymbol{t})+\boldsymbol{\Delta f_p}(\vec{\boldsymbol{x}},\boldsymbol{t})$$

where

$$\boldsymbol{f_p^{eq}}=\boldsymbol{w_p n}\left[\boldsymbol{1}+\boldsymbol{3}\vec{\boldsymbol{u}}\cdot\vec{\boldsymbol{c}}_{\boldsymbol{p}}+\left(\boldsymbol{9}\left(\vec{\boldsymbol{u}}\cdot\vec{\boldsymbol{c}}_{\boldsymbol{p}}\right)^{\boldsymbol{2}}-\boldsymbol{3u^2}\right)/\boldsymbol{2}\right]$$

represents the discrete Maxwell-Boltzmann equilibrium, associated to the weight w_p and discrete speed $\vec{c}_p$. In addition

$$\boldsymbol{n}=\textstyle\sum_{\boldsymbol{p}}\boldsymbol{f_p}\text{ and }\vec{\boldsymbol{u}}=\sum_{\boldsymbol{p}}\vec{\boldsymbol{c}}_{\boldsymbol{p}}\boldsymbol{f_p}\,/\boldsymbol{n}$$

are the plasma density and velocity, respectively. The term Δf_p is proportional to

$$\vec{\boldsymbol{G}}=-\boldsymbol{\gamma}\textstyle\sum_{\boldsymbol{i}}(\vec{\boldsymbol{V}}_{\boldsymbol{i}}-\vec{\boldsymbol{u}})\boldsymbol{\delta}(\vec{\boldsymbol{x}}-\vec{\boldsymbol{R}}_{\boldsymbol{i}}),$$

the drag force exerted by the plasma on the red blood cell located at position $\vec{R}_i$ and having velocity $\vec{V}_i$, via the coefficient γ, and vice versa. The drag force is bidirectional and couples plasma and red blood cells according to the action-reaction principle.

Stationary flow conditions are simulated at 45% hematocrit and in diastole (maximal flux) conditions, corresponding to inflow velocity of 0.9 m/s at the coronary inlet (i.e., from the aorta). At the inlet the imposed boundary condition are either the flow rate or the pressure and at the outlets the pressure is imposed. At first, the pressures at the different outlets are taken to be equal, that is, without considering a specific peripheral resistance. Additional simulations were based on a peripheral resistance model via a Windkessel (WK) feedback where the portion of myocardium subtended by each outlet is modeled as a peripheral resistance R_{per}, being taken equal for all outlets. The outlet pressures are adjusted once Q, the instantaneous flow rate at the outlet, is determined during simulation. In the protocol, the outlet pressure is adjusted cyclically as $p_{out}^{(n)}=p_v+R_{per}Q^{(n)}$, where p_v is the venous pressure, until convergence to steady-state is reached.

Reference inflows for the different cases are unknown a priori. Therefore, we preliminarily simulate two regimes of the inflow, corresponding to Reynolds number of 10 and 200, subsequently we simulated the system at Reynolds 100, with and without the peripheral resistance model. The conditions of variable Reynolds number expose viscous and inertial effects respectively, and allow inspecting the role of the flow rate on the pressure losses. FFR is computed by considering the aortic/inlet pressure p_a and the distal pressure p_d, so that $\text{FFR}=\frac{p_d}{p_a}$. FFR measurement variability on FFR-guided treatment strategy has shown that a cutoff of FFR<0.80 indicates clinically useful PCI, with a gray-zone found between 0.75% and 0.85%. Therefore clinicians typically make revascularization decisions based on broadened clinical judgment when a single FFR falls within the uncertainty range. We estimate the severity of a stenosis as $s=\left(\frac{d_n-d_s}{d_n}\right)\times 100\%$ where d_n and d_s are the vessel diameter in the stenotic and healthy proximal region of the artery, respectively. Pressure losses depend critically on the Reynolds number, defined as $Re=u_pD/\nu$, where u_p is the proximal flow velocity, D the vessel diameter at the inlet, and ν is the kinematic viscosity which depends intrinsically on the hematocrit.

In this study, the distal points were located downstream and near the visible stenoses, such locations were assigned based on a reasonability criterion. In order to compare the data with the clinical ones, we estimate a systematic error of 5% on the measured FFRs. For case P1 the left coronary artery presents a diffused stenosis along the LAD segment. The left coronary artery of P2 presents a marked localized stenosis on the LCX segment, proximal to the LCX/OM bifurcation. The right coronary artery of case P3 presents a marked diffused stenosis distal to the first bifurcation. Case P4 presents a mild stenosis on the LAD segment, proximal to the bifurcation with LCX and near the aorta region (inlet). High-performance simulations were performed with the MUPHY software [9].

In vitro measurements providing a first direct and independent assessment of the hemodynamic flow in a faithful reproduction of the coronary arteries are currently under way. To this purpose, the experimental coronary model is made in silicon rubber, namely transparent in order to allow the optical access. The 3D prototype employed for the realization of the elastic model is achieved from the same CT scans as used in simulation: after the segmentation of the clinical images obtained by using the software MUPHY, the anatomically accurate replica of the coronary artery tree is realized by means of the Fused Deposition Modeling (FDM) Technology, i.e. a professional 3D printing technology. The ratio between *in vitro* and in silico geometries is 4:1.

To fulfill the dynamical similarity, the two non-dimensional numbers, the Reynolds and the Womersley number, defined $\mathrm{Wo} = \sqrt{\mathrm{D}^2/\mathrm{T}\nu}$ where T is the period of the cardiac cycle, are chosen to be equal between experiments and simulations. The fluid dynamics analysis is performed in pulsatile flow testing already used in previous investigations [10-14] at varying heart rate and stroke volume conditions (i.e. at different Reynolds). Reproducing the mock circulatory system for pulsatile flow studies is not easy: in fact the flow in the cardiovascular system is pulsatile and three-dimensional, the anatomic geometry is complex and also the larger arteries adapt to varying flow and pressure conditions by expanding and contracting. To overcome these difficulties, the experimental activities are performed in the Pulse Duplicator i.e. a hydraulic loop simulating the human systemic circulation in both flow rate and ventricular-aortic pressure waves. A positive displacement piston pump moves accordingly to a given pulsatile time function governing the volume changes of the ventricle. The coronary artery trees, which are the core of the apparatus, are placed in a plexiglass container and made of silicon rubber, in order to both simulate the physiological blood vessel elasticity, and also for the optical access required for the experiments.

The flow pattern is reconstructed by evaluating both the velocity and pressure fields. To perform the 2D velocity measurements the working fluid (distilled water) is seeded with neutrally buoyant particles (dp~30 μm). The central plane of the coronary tree is illuminated by a 12 W infrared laser and the high-speed digital camera recorded the movies at 500 frames/s, 1280x1024 pixel resolution. A Feature Tracking algorithm [10] developed to be optimal for complex, non-steady flows under investigation, is used to recognize particles trajectories. Interpolation of data on a regular 50x51 grid then gave the 2-D velocity matrix. Spatio-temporal resolution (Δx_{min}=1.45 mm Δt_{min}=1/500 s) is high enough to identify the structures. The flow rate is monitored by using an electromagnetic flow meter. Finally, the pressure fields and the local pressure change evaluated across the stenosis are recorded by means of two piezoelectric sensors (PCB Piezotronics® 1500 series) placed before and after the stenotic plaques.

3. RESULTS

The FFRs obtained from the computer simulations are reported in Figure 2. The pressure distribution shows abrupt variations in proximity of the stenotic regions. Among the four cases, pressure losses are more visible for the P2 and P3 cases, in particular for P2 presenting a stenotic severity above 50%. In general, the behavior of the segmentation and simulation protocol provide stable and the results depend weakly on modifications of the segmentation and filtering of the imaging data. In general, the trend in the clinical FFR is well reproduced by the simulations with the computer-reconstructed data shows a significant dependence on the flow rate (see Figure 3). By tuning the latter, we empirically found that Re=100 represents the value with optimal agreement with the clinical data.

The agreement between clinical and computational FFR is less satisfactory for case P1 and case P4. For case P1, the origin of the disagreement should be found in the large pressure drops that arise from the small proximal arterial bifurcations that reduce significantly the flow rate along the main stenosis. By accounting for the peripheral resistance, the pressure drop is reduced significantly at the proximal bifurcations and increases with the flow rate. For case P4 the vicinity to the inlet renders the result somehow dependent on the boundary region since the entrance length interferes with the measured FFR. The best agreement is found for cases P2 and P3, where distal bifurcations and a safe distance from the inlet mitigate the above conditions. For cases P1, P3 and P4 the usage of a peripheral resistance model further ameliorates the agreement between the computed and clinical data.

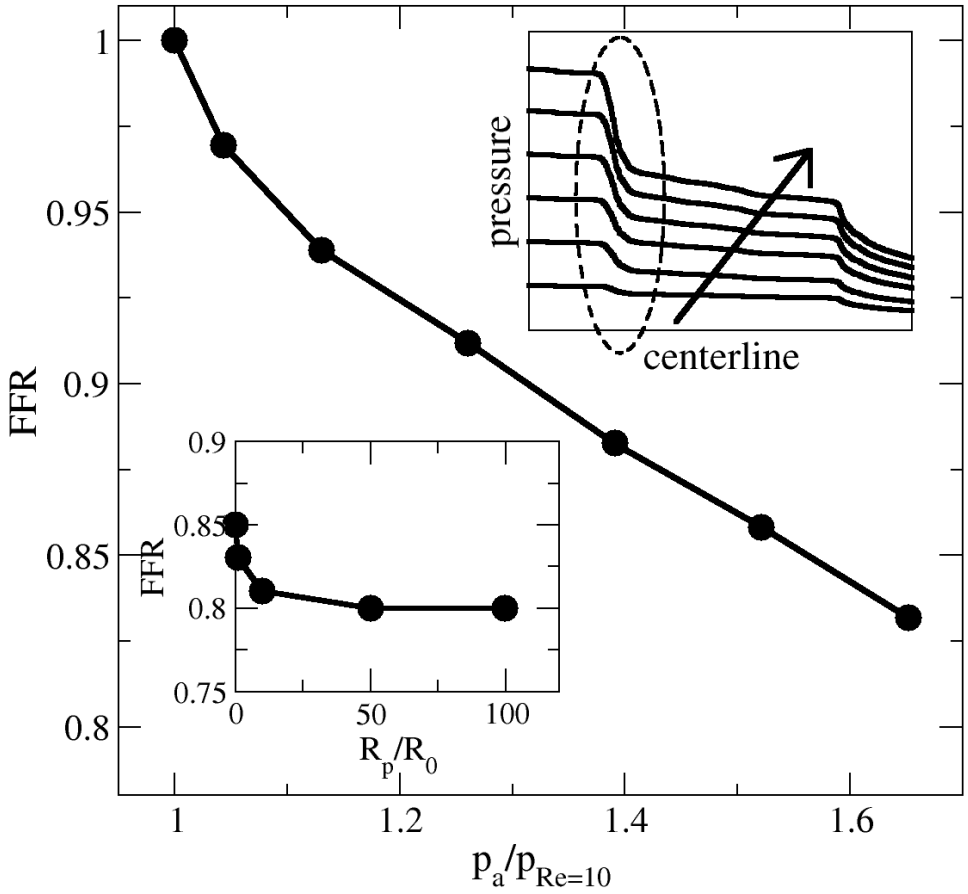

Figure 3: FFR for case P1 versus the imposed pressure. Data collected for the model with the resistive periphery and $p_{Re=10}$ refers to the aortic pressure corresponding to Re=10. Lower inlet: FFR vs the imposed peripheral resistance R_p, with R_0 being the estimated resistance of the LAD vessel. Upper inlet: time-averaged pressure profiles along the vessel centerline in correspondence to the main stenosis (marked by the ellipse) and followed by a second smaller stenosis. The arrow shows the ordering of profiles at increasing inlet pressure.

Figure 3 shows the dependence of FFR on the imposed aortic pressure for the P1 case and by employing a resistive periphery. Changing the inlet pressure modulates the local flow velocity u and, as the pressure drop has both viscous and inertial origin, the pressure drop increases with the flow velocity as $\Delta p = au + bu^2$, with a resulting $FFR = 1 - a - bu$. The linear behaviour is exhibited in Figure 3 already for a mild value of the inlet pressure, ensuring the dominance of the inertial loss. By analyzing the parametric effect of the peripheral resistance in all four cases we also notice a mild yet visible effect on FFR. This is partially expected, as changing the pressures at the outlets corresponding to the small branches proximal to the stenosis, a substantial rerouting of the flow in the stenotic branch takes place. However, flow rerouting has an effect smaller than 6% for all four cases on the computed FFR, which in turns has repercussions for decision-making given the similar extent of the FFR gray-zone.

4. CONCLUSIONS

The proven clinical value of FFR is based on the identification of individual coronary arteries that will benefit from revascularization, such as percutaneous coronary intervention. The functional importance of vessel stenoses on coronary hemodynamics is made possible by reproducing the flow pattern in an accurate anatomical reconstruction based on tomographic data.

The results on FFR obtained through computer simulations provide close similarity with clinical data. In particular, by tuning the hemodynamic flow to an effective Reynolds of 100 provide good agreement with clinical data. In absence of other sources of information on the flow rate, such value can be seen as a good parameter to reproduce FFR during maximal hyperemia. Adopting a resistive model is a necessary step in order to mimic the peripheral vasculature, employed here as a boundary condition for the hemodynamics explicitly solved in three-dimensional space. However, the employed peripheral resistance should faithfully reproduce the amount of myocardium territory subtended by the different vessels, the role of collateral circulation, the right extent of hyperemic conditions, and any other source of physiological auto-regulation. Our data showed that based on a simplified version of the periphery, the computer reconstructed FFR presents a better match with the clinical values and, in addition, has a weak, yet non-marginal, dependence on the resistive parameter.

These indications calls for an in-depth analysis based on more sophisticated models of the microvasculature, some of which are currently under investigation. The relevance of the presented results is the good reproducibility of the clinical data, posing the basis for a more systematic and joint *in vitro* / in silico studies on a larger set of patients.

REFERENCES

[1] De Bruyne, B.and Sarma, J., "Fractional flow reserve: a review," Heart 94, 949-959 (2008).

[2] Leone, A. M. , Porto, I., De Caterina, A. R., Basile, E., Aurelio, A., Gardi, A., Russo, D., Laezza, D., Niccoli, G., Burzotta, F., Trani, C., Mazzari, M. A., Mongiardo, R., Rebuzzi, A. G and Crea, F., "Maximal hyperemia in the assessment of Fractional Flow Reserve," JACC: cardiovascular intervention 5(4), 402-408 (2012) .

[3] Leone, A. M., De Caterina, A. R., Basile, E., Gardi, A., Laezza, D., Mazzari, M. A., Mongiardo, R., Kharbanda, R., Cuculi, F., Porto, I., Niccoli, G., Burzotta, F., Trani, C., Banning, A. P., Rebuzzi, A. G. and Crea, F., "Influence of the amount of Myocardium subtended by a stenosis on Fractional Flow Reserve," Circ. Cardiovasc. Interv. 6 (1), 29-36 (2013).

[4] Melchionna, S., Amati, G., Bernaschi, M., Bisson, M., Succi, S., Mitsouras, D. and Rybicki, F. J., "Risk assessment of atherosclerotic plaques based on global biomechanics,". Med. Eng. & Phys. 35 (9), 1290-1297 (2013).

[5] Zarins, C. K., Taylor C.A. and Min, J. K., "Computed Fractional Flow Reserve (FFT_{CT}) derived from coronary CT angiography," J. Cardiovasc. Trans. Res. 6, 708-714 (2013).

[6] Taylor, C. A., Fonte, T. A. and Min, J. K., "Computational fluid dynamics applied to cardiac computed tomography for noninvasive quantification of fractional flow reserve: scientific basis," J. Am. Coll. Cardiol. 61(22), 2233-2241 (2013).

[7] Melchionna, S., Bernaschi, M., Succi, S., Kaxiras, E., Rybicki, F. J., Mitsouras, D., Coskun, A. U. and Feldman, C. L., "Hydrokinetic approach to large-scale cardiovascular blood flow," Comput. Phys. Comm. 181(3), 462-472 (2010).

[8] Melchionna, S., "A model for red blood cells in simulations of large-scale blood flows," Macromol. Theory & Simul. 20(7), 548-561 (2011).

[9] Bernaschi, M., Melchionna, S., Succi, S., Fyta, M., Kaxiras, E. and Sircar, J. K., "MUPHY: a parallel MUlti PHYsics/scale code for high performance bio-fluidic simulations," Comput. Phys. Comm. 180(9), 1495-1502 (2009).

[10] Cenedese, A., Del Prete, Z., Miozzi, M. and Querzoli, G., "A laboratory investigation of the flow in the left ventricle of a human heart with prosthetic, tilting-disk valves," Exp. Fluids 39(2) 322-335 (2005).

[11] Querzoli, G., Fortini, S. and Cenedese, A., "Effect of the prosthetic mitral valve on vortex dynamics and turbulence of the left ventricular flow," Phys. Fluids 22, 041901-041910 (2010).
[12] Vukicevic, M., Fortini, S., Querzoli, G., Espa, S. and Pedrizzetti, G., "Experimental Study of an Asymmetric Heart Valve Prototype," Eur. J. Mech. B-Fluid. 35, 54-60 (2012).
[13] Espa., S., Badas, M. G., Fortini, S., Querzoli, G. and Cenedese, A., "A Lagrangian Investigation of the flow inside the left ventricle," Eur. J. Mech. B-Fluid. 35, 9-19 (2012).
[14] Fortini, S, Querzoli, G, Espa, S. and Cenedese, A., "Three-dimensional structure of the flow inside the left ventricle of the human heart," Exp. Fluids 54, 1609 (2013).

The present work has not been submitted for publication or presentation elsewhere.